AMERICAN SOCIETY FOR MICROBIOLOGY | Journal of Virology®

STRUCTURE AND ASSEMBLY

# Increased Epitope Complexity Correlated with Antibody Affinity Maturation and a Novel Binding Mode Revealed by Structures of Rabbit Antibodies against the Third Variable Loop (V3) of HIV-1 gp120

**Ruimin Pan,[a] Yali Qin,[b] Marisa Banasik,[b] William Lees,[c] Adrian J. Shepherd,[c] Michael W. Cho,[b] Xiang-Peng Kong[a]**

[a]Department of Biochemistry and Molecular Pharmacology, NYU School of Medicine, New York, New York, USA

[b]Department of Biomedical Sciences, Iowa State University, Ames, Iowa, USA

[c]Institute of Structural and Molecular Biology, Birkbeck College, University of London, London, United Kingdom

**ABSTRACT** The third variable (V3) loop of HIV-1 gp120 is an immunodominant region targeted by neutralizing antibodies (nAbs). Despite limited breadth, better characterization of the structural details of the interactions between these nAbs and their target epitopes would enhance our understanding of the mechanism of neutralization and facilitate designing better immunogens to induce nAbs with greater breadth. Recently, we isolated two anti-V3 neutralizing monoclonal antibodies (MAbs), 10A3 and 10A37, from a rabbit immunized with gp120 of the M group consensus sequence. In this study, crystal structures of these MAbs bound to target epitopes were determined. 10A3 binds to the V3 crown ($^{303}$TRKSIHIGPGRAF$^{317}$) using the cradle binding mode, similar to human V3 MAbs encoded by IGHV5-51 germ line genes, and its epitope structure resembles that bound to the human antibodies. In contrast, 10A37, which exhibits greater breadth and potency than 10A3, binds the V3 crown and the succeeding stem region ($^{308}$HIGPGRAFYTTGEI$^{323}$). Unexpectedly, the $^{315}$RAFYTT$^{320}$ portion of the epitope existed as helical turns, a V3 structure that has not been observed previously. Its main chain-dominated antigen-antibody interactions not only explain the broad neutralization of 10A37 but also show that its epitope is a potential vaccine target to be further evaluated. In conclusion, our study provides novel insights about neutralization-susceptible epitope structures of the V3 loop of HIV-1 gp120 and demonstrates that, despite low amino acid sequence similarity to human antibody germ line genes, rabbits can serve as a useful animal model to evaluate human vaccine candidates.

**IMPORTANCE** The apex crown of V3 of HIV-1 gp120 is the most immunogenic region of the surface glycoprotein, and many MAbs targeting this region have been developed. Structural understanding of V3 crown MAbs not only can help understand how antibody responses target this unique region but also contribute to immunogen design for vaccine development. We present here crystal structures of two neutralizing V3 MAbs, 10A3 and 10A37, developed from a rabbit immunized with gp120. Our analysis of 10A3 in complex with V3 provided a detailed example of how epitope complexity can evolve with affinity maturation, while that of 10A37 revealed a novel V3 binding mode targeting the C-terminal side of the V3 crown and showed that this region can form a helical structure. Our study provides novel insights about neutralization-susceptible V3 epitope structures and demonstrates that rabbits can serve as a useful animal model to evaluate human vaccine candidates.

**KEYWORDS** HIV-1, gp120, V3 loop, neutralizing antibody, V3

**Received** 31 October 2017 **Accepted** 10 January 2018

**Accepted manuscript posted online** 17 January 2018

**Citation** Pan R, Qin Y, Banasik M, Lees W, Shepherd AJ, Cho MW, Kong X-P. 2018. Increased epitope complexity correlated with antibody affinity maturation and a novel binding mode revealed by structures of rabbit antibodies against the third variable loop (V3) of HIV-1 gp120. J Virol 92:e01894-17. https://doi.org/10.1128/JVI.01894-17.

**Editor** Wesley I. Sundquist, University of Utah



Address correspondence to Michael W. Cho, mcho@iastate.edu, or Xiang-Peng Kong, xiangpeng.kong@med.nyu.edu.

The third variable (V3) loop of gp120 plays a critical function in viral entry into host cells. It determines viral tropism by binding coreceptor CCR5 or CXCR4 (1–4). Linked by a disulfide bond between residues 296 and 331 (HXB2 numbering) (5), it is almost always 35 amino acids in length. Structurally, the V3 loop can be divided into 3 regions: the crown (residues 304 to 318), the stem, and the base regions (6). Despite being variable in sequence, the crown region is structurally quite conserved, and it often forms a beta hairpin (6–9). The V3 loop is highly immunogenic (10–13) and induces mostly strain-specific neutralizing antibodies (nAbs). High levels of antibodies targeting the V3 loop have also been detected in animals vaccinated with gp120 or V3 peptides (14–18). Many V3 crown-specific monoclonal antibodies (MAbs) have been isolated from HIV-1-infected patients (11, 19), and a number of Fab/epitope complex structures of them have been determined (8, 20–26), setting the foundation for understanding the structural basis of Ab responses against the V3 crown. Sieve analyses of the RV144 clinical trial indicated that the V3 loop of HIV-1 envelope glycoprotein gp120-specific antibodies correlated with a reduced risk of infection (27, 28), indicating the V3 loop is a target for HIV vaccine design.

The antigen binding modes of human V3 crown MAbs have been shown to fall largely into two general categories: cradle or ladle binding modes (8, 24, 25). In the cradle mode, the V3 crown lies along an antigen binding groove resembling a cradle. In the ladle mode, the Ab has a long-standing complementarity-determining region (CDR) H3 (the handle of the ladle), which interacts with the main chain of the N-terminal beta strand of the V3 crown and a pocket at the base of the CDR H3 (the bowl of the ladle), which interacts with the apex turn of the V3 crown. Data suggested that human V3 crown Abs preferentially use IGHV5-51 germ line genes (19), and such Abs (e.g., MAb 2557) use the cradle binding mode (8, 25). IGHV3 germ line genes are also frequently used, and some IGHV3-encoded V3 crown Abs (e.g., MAbs 447-52D and 537-10D) use the ladle binding mode (21, 24, 29, 30). In both binding modes, the N-terminal strand of the V3 crown plays a key role in the antibody-antigen interaction. In the cradle binding mode, the N-terminal strand of the V3 crown is buried deep in the antigen binding groove while the C-terminal residues make additional contacts with the antibody. In the ladle binding mode, the N-terminal strand of the V3 crown interacts with CDR H3 of the antibody, and the C-terminal residues are not always observable in the complex structures, indicating there is no or very little contact with the antibody. MAbs isolated from small animals immunized with V3 peptides or monomeric gp120 have been shown to be able to mimic human MAb binding modes (26). For example, rabbit MAb R56 and mouse MAb 50.1 preferentially recognize the V3 crown, similar to the cradle binding mode used by human Abs encoded by IGHV5-51 germ line genes (20, 26). However, the epitopes of these MAbs are shorter and less complex than that of human Ab developed from infected patients, and their evolution with affinity maturation is not understood.

We have recently isolated a panel of new V3 loop-specific MAbs from a rabbit immunized with gp120 based on the M group consensus sequence (MCON6), and two of them, 10A3 and 10A37, exhibited neutralizing activities (16). They target different regions of the V3 loop: 10A3 recognizes a peptide consisting of residues RKSIRIGPGQAFYAT (amino acids [aa] 304 to 320), and 10A37 recognizes a peptide consisting of residues RIGPGQAFYATGDII (aa 308 to 324), atypical for V3 MAbs. Interestingly, they also competed with PGT121, one of the broadly neutralizing MAbs targeting the V3 base glycan patch (16, 31). To precisely define the epitopes of these two MAbs and characterize their antigen-antibody interactions at the atomic level, we determined their Fab/epitope complex structures and compared them with V3-specific rabbit MAb R56 (26) and human V3-specific MAbs derived from the IGHV5-51 germ line gene (8, 25). The results showed that MAb 10A3 targets the V3 crown, similar to rabbit MAb R56, but makes additional contacts with the C terminus of the V3 crown region, correlating with additional somatic hypermutations. The cradle antigen binding mode of 10A3 is similar to those of human V3-specific MAbs derived from the IGHV5-51 gene. In contrast, 10A37 targeted the V3 crown and the succeeding stem region in a new binding mode not observed previously, and its V3 epitope harbors a helix core.

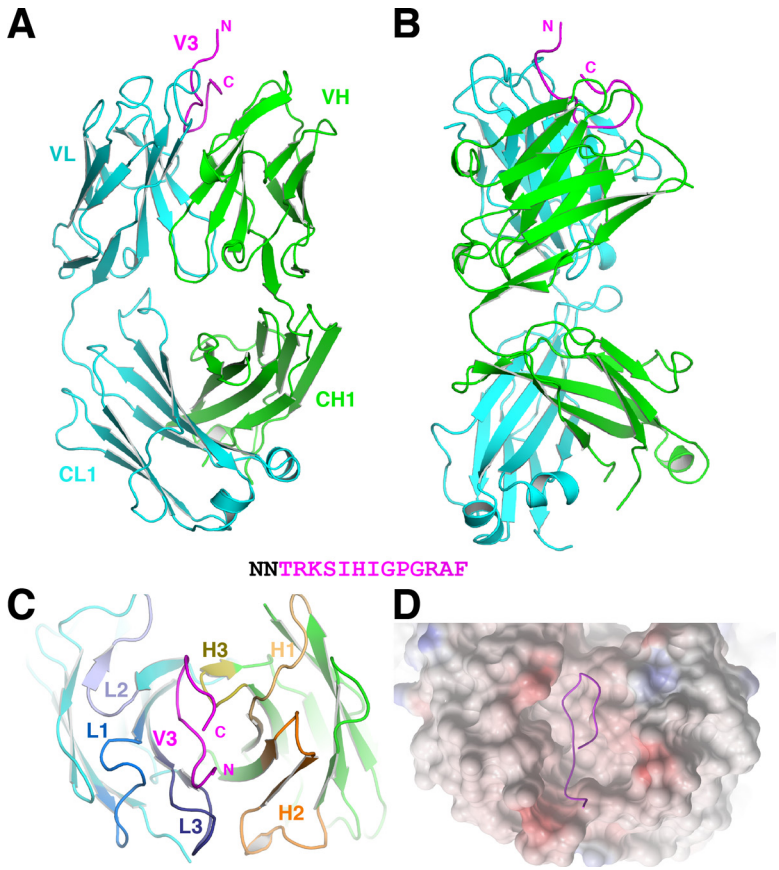


**FIG 1** Structure of Fab 10A3 in complex with $V3_{ConB}$. (A and B) Ribbon representations of the Fab 10A3 in complex with $V3_{ConB}$ from two different perspectives. The light and heavy chains are colored cyan and green, respectively, while the epitope is colored magenta (the coloring scheme is the same for all figures, except where indicated otherwise). (C) The antigen binding site of 10A3, with the CDR loops labeled and colored differently from the rest of Fab. (D) Electrostatic potential surface of the antigen binding site of 10A3, with red color indicating negatively charged while blue indicates positively charged. (Inset) The sequence of the peptide used for crystallization is shown, and residues observed in the electron density map are shown in magenta.

This study provides novel insights about neutralization-susceptible epitope structures of the V3 loop of gp120 and further discerned that rabbit is a useful animal model for the evaluation of the immunogenicity of vaccine candidates.

## RESULTS

**Determination of the complex structure of 10A3/$V3_{ConB}$.** MAb 10A3 is a chimeric antibody with a rabbit variable region and human constant region. The peptide used for cocrystallization was selected by screening from a panel of V3 peptides already available by ELISA based on the epitope mapping results (16). 10A3 Fab was cocrystallized with a 15-mer clade B consensus V3 peptide ($V3_{ConB}$; NNTRKSIHIGPGRAF), which differs from MCON6 gp120 immunogen only at residue 315 (NNTRKSIHIGPGQAF), which does not play a key role in antibody binding (see below). The crystal of the complex belongs to orthorhombic space group $P2_122_1$, and the complex structure was determined by molecular replacement and refined to 1.9-Å resolution (Fig. 1 and Table 1). As there is only one complex in the asymmetry unit, we assigned the chain identities of the light and heavy chains and the peptide epitope as L, H, and P, respectively. Amino acid residues on the light and heavy chains were numbered according to the Kabat and Wu convention (32), and V3 residues were numbered based on the HXB2 scheme. A residue is referred to by its number preceded by its chain identifier; for example, $Arg^{P315}$ refers to arginine residue 315 of the peptide epitope. Thirteen V3 residues ($^{303}$TRKSIHIGPGRAF$^{317}$) were observed in the electron density map and have been built into the final structure.

**TABLE 1** Crystallographic data collection and refinement statistics[a]

| Parameter | Fab 10A3/V3$_{ConB}$ | Fab 10A37/V3$_{JR-FL}$ |
|---|---|---|
| Data collection | | |
| Space group | $P2_122_1$ | $P2_1$ |
| Cell dimensions | | |
| *a*, *b*, *c* (Å) | 62.85, 83.87, 90.61 | 43.23, 173.90, 70.91 |
| $\alpha$, $\beta$, $\gamma$ | 90.00, 90.00, 90.00 | 90.00, 99.98, 90.00 |
| Resolution (Å) | 1.90 (2.01–1.90) | 2.55 (2.70–2.55) |
| CC (1/2)[b] | 100.0 (94.1) | 99.6 (83.0) |
| $R_{sym}$ | 6.5 (46.8) | 10.0 (54.6) |
| $I/\sigma I$ | 31.1 (5.1) | 11.9 (3.0) |
| Completeness (%) | 99.8 (98.8) | 99.2 (98.6) |
| Redundancy | 13.3 (10.4) | 4.3 (4.3) |
| Refinement | | |
| Resolution (Å) | 39.86–1.90 | 44.61–2.55 |
| No. of unique reflections | 38,386 | 33,251 |
| $R_{work}/R_{free}$ | 17.85/22.43 | 20.61/25.21 |
| No. of atoms | | |
| Protein | 3,312 | 6,622 |
| Solvent | 668 | 227 |
| Avg B factor (Å$^2$) | 28.0 | 45.2 |
| RMSD | | |
| Bond length (Å) | 0.006 | 0.008 |
| Bond angle (°) | 0.855 | 1.049 |
| PDB code | 5V6M | 5V6L |

[a]Statistics in parentheses refer to the outer resolution shell.
[b]CC (1/2), percentage of correlation between intensities from random half data sets.

The complex structure of 10A3/V3$_{ConB}$ shows that 10A3 binds the V3 crown by using the cradle binding mode. The antigen binding pocket is deep and shaped like a cradle, with the third complementarity-determining regions (CDRs) of the light and heavy chains (L3 and H3) situated at each end of the cradle (Fig. 1 and 2) and CDRs H1 and H2 forming a wall on one side of the peptide while CDRs L1 and L2 were on the other side. The periphery of the cradle is negatively charged, contributed by Glu$^{L50}$ (L2) and Asp$^{L93}$ (L3) of the light chain on one side and Asp$^{H53}$ (H2) of the heavy chain on the other side (Fig. 1D and 2A). The bottom of the cradle is hydrophobic, contributed by Ala$^{L91}$, Leu$^{L89}$ Phe$^{L94}$, Phe$^{H96}$, and a disulfide bond between Cys$^{H35}$ and Cys$^{H50}$ near CDR H2. Such CDR loop disulfide bonds are rarely observed in human Abs but quite frequently in rabbit ones (26, 33).

**Detailed antigen-antibody interactions of 10A3/V3$_{ConB}$.** The antigen-antibody interactions of 10A3 buried a total of 969 Å$^2$ of surface area, with 475 Å$^2$ from the antibody and 494 Å$^2$ from the antigen, involving both hydrophilic and hydrophobic ones.

**(i) The hydrophilic interactions.** The side chains of epitope residues Arg$^{P304}$ and His$^{P308}$ interact directly with negatively charge residues of 10A3 at the periphery of the cradle. Specifically, the N-terminal Arg$^{P304}$ forms a salt bridge with Asp$^{H53}$ (from CDR H2), and its side chain also stacks with the benzyl group of Phe$^{P317}$ that can stabilize its orientation. His$^{P308}$ also forms a potential salt bridge with Glu$^{L50}$ (L2). Additionally, Ser$^{P306}$ can form hydrogen bonds with the side chain of Asn$^{L32}$ (L1) and the carbonyl group of Tyr$^{L28}$ (L1). The side chain of Asn$^{H95}$ forms a hydrogen bond with the carbonyl oxygen of His$^{P308}$, and it has the biggest contact area (~50Å$^2$) with the epitope among residues of the heavy chain or the whole antibody.

**(ii) The hydrophobic interactions.** Several highly conserved residues, including Ile$^{P307}$, Ile$^{P309}$, and Pro$^{P313}$, of the V3 crown play key roles in the hydrophobic interactions. Ile$^{P307}$ and Ile$^{P309}$ are buried in a hydrophobic pocket, and the residues of 10A3 that contribute these hydrophobic interactions are Ala$^{H33}$ (H1), Cys$^{H50}$ and Ala$^{H52}$ (H2), and Leu$^{L89}$, Ala$^{L91}$, and Phe$^{L94}$ (L3). Pro$^{P313}$ stacks with two aromatic side chains of Tyr$^{H97}$ and Tyr$^{L49}$ (Fig. 2C). Although 10A3 has a very short four-residue CDR H3 (NFYL; Kabat definition), it plays several important roles in antigen binding. In addition, Phe$^{H96}$

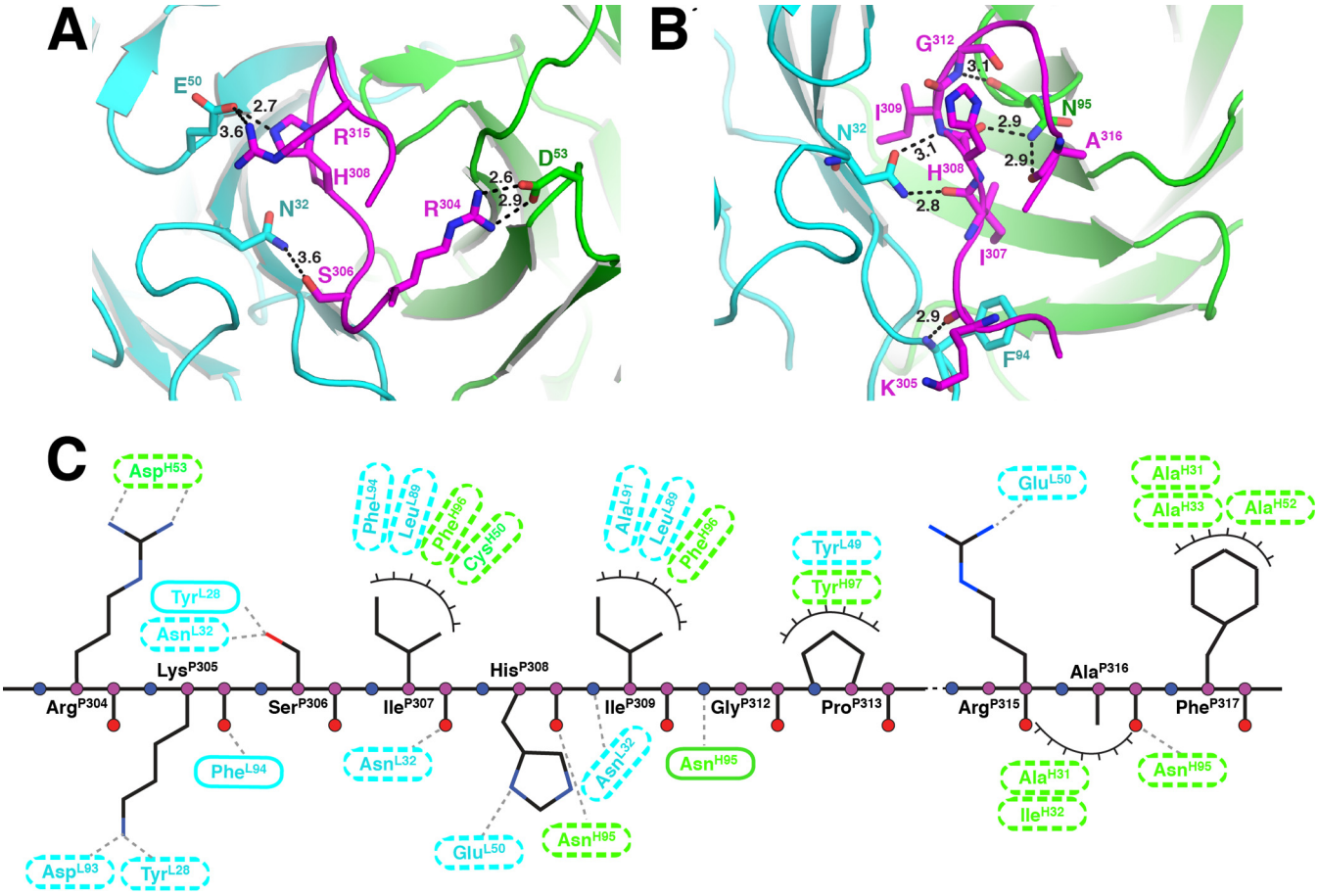


**FIG 2** Antigen-antibody interactions of 10A3/$V3_{ConB}$. (A) Hydrophilic interactions between the side chains of the epitope and residues of 10A3. (B) Hydrophilic interactions between the main chain of the epitope and residues of 10A3. (C) Schematic illustration of antigen-antibody interactions. Hydrogen binding interactions are indicated by dashed lines between the residues, while van der Waals contacts are indicated by eyelashes. Residues in solid ovals contribute to the interactions by their main-chain atoms, and those in dashed ovals contribute to their side-chain atoms.

contributes to the hydrophobic pocket, burying the two conserved isoleucines $Ile^{P307}$ and $Ile^{P309}$ of V3, and $Tyr^{H97}$ stacks with $Pro^{P313}$ in the arch region of V3. Notably, the backbone of the epitope is also involved extensively in binding the antibody, and there are six contacts between the backbone of V3 and 10A3 (Fig. 2B and C). Another point is that the side chain of the signature residue $Arg^{P315}$ (which would be Gln in non-clade B strains) points away from the antigen binding site, even though it can form a salt bridge with $Glu^{L50}$ (3.6 Å).

**Determination of the complex structure of 10A37/$V3_{JR-FL}$.** The Fab of rabbit MAb 10A37, which has a better potency and breadth of neutralizing activity than 10A3 does (16), was cocrystallized with a 23-mer JR-FL V3 peptide, NNTRKSIHIGPGRAFYTTGEIIG ($V3_{JR-FL}$; residues 301 to 325); its sequence differs from that of MCON6 immunogen at two positions (NNTRKSIHIGPGQAFYATGEIIG). The complex structure was also determined by molecular replacement and refined to 2.3-Å resolution (Fig. 3 and Table 1). The crystal of the complex belongs to monoclinic space group $P2_1$, and there are two essentially identical Fab/V3 complexes in the asymmetry unit (V3 epitope C$\alpha$ root mean squared deviations [RMSD], 0.3Å). For simplicity, only one complex is used here, and the residues are numbered as mentioned above for the 10A3/$V3_{ConB}$ complex, using L, H, and P to denote light chain, heavy chain, and V3, respectively. Sixteen residues of V3, from 308 to 323, with sequence HIGPGRAFYTTGEI, were observed in the electron densities and have been built into the final structures (Fig. 3 and 4). It is clear that 10A37 has a new mode of binding the V3 crown, different from those that have described previously (8, 24, 25, 34). Surprisingly, the epitope of 10A37 has a helix core ($^{315}$RAFYTT$^{320}$), with the N terminus of

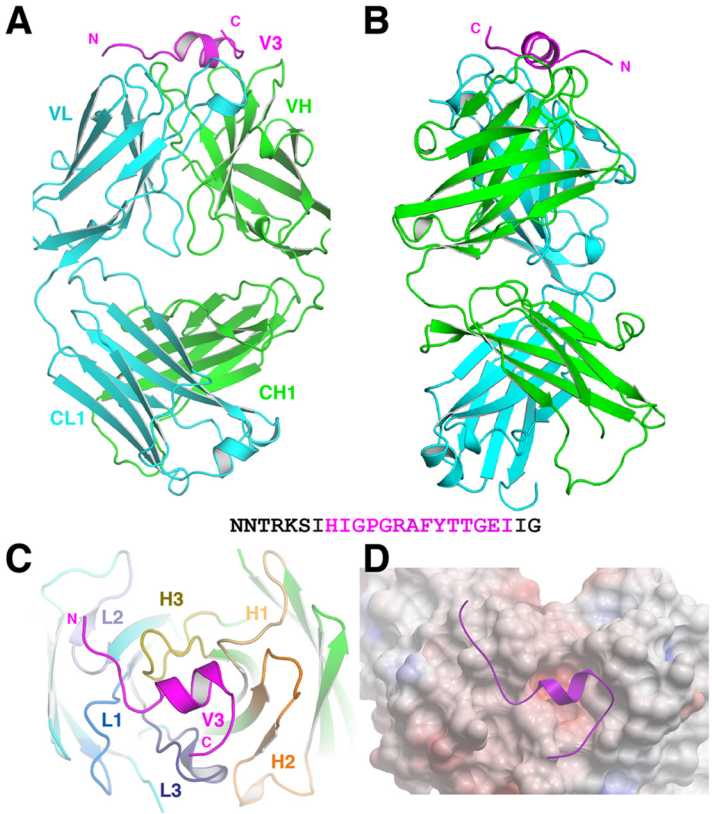


**FIG 3** Structure of Fab 10A37 in complex with $V3_{JR-FL}$. (A and B) Ribbon representations of the Fab 10A37 in complex with $V3_{JR-FL}$ from two different perspectives. (C) The antigen binding site of 10A37 with the CDR loops labeled and colored differently from the rest of Fab. (D) Electrostatic potential surface of the antigen binding site of 10A37. (Inset) The sequence of the peptide used for crystallization is shown, and residues observed in the electron density map are shown in magenta.

the epitope extending straight out on one side of the helix core and the C terminus bent back on the other side. A circular dichroism experiment using a full-length cyclic V3 (JR-FL sequence) revealed that it has weakly helical conformation (not shown), suggesting that some region of V3 has an intrinsic propensity for a helical conformation. Interestingly, the heavy chains of 10A3 and 10A37 are derived from the same rabbit germ line gene, IGHV1S45*01 (15), but their CDR H3 lengths are very different: 4 versus 12 residues (Kabat definition), respectively.

**Detailed antigen-antibody interaction of 10A37/$V3_{JR-FL}$.** The antigen-antibody interactions buried a total surface area of 723 Å$^2$, contributed equally from the antibody and the V3 epitope. There are two pockets on the surface of 10A37 antigen binding site (Fig. 3D): one is ~10 Å deep, burying the side chains of $Phe^{P317}$ and $Tyr^{P318}$ from the helix core, and another one is shallow, accommodating $Pro^{P313}$ before the helix. The side chain of $Ile^{P323}$ is also half buried at the edge of the deep pocket. Again, we can divide the antigen-antibody interactions into hydrophilic and hydrophobic ones.

**(i) Hydrophilic interactions between the side chains of V3 residues and 10A37.** At the bottom of the deep pocket, $Asp^{H95}$ (of CDR H3) is buried by the side chain of $Tyr^{P318}$; the OH group of $Tyr^{P318}$ is located between an OD atom of $Asp^{H95}$ (2.75Å) on one side and the OH of $Tyr^{L93}$ (L3; 2.54Å) on the other side (Fig. 4A). The side chain of $His^{P308}$ at the N-terminal end of the epitope can also form a hydrogen bond with the OH group of $Tyr^{H100A}$ (H3).

**Hydrophobic interactions.** As mentioned already, $Phe^{P317}$ and $Ile^{P323}$, in addition to $Tyr^{P318}$, are buried in a hydrophobic pocket, formed by $Phe^{H34}$ (H1), $Tyr^{H58}$ (H2), and $Try^{L93}$ and $Ile^{L95D}$ (L3). The aromatic plane of $Phe^{P317}$ is on top of $Phe^{H34}$ and $Try^{L93}$, while the side chain of $Ile^{P323}$ is on top of $Tyr^{H58}$ and $Ile^{L95D}$. The V3 arch residue $Pro^{P313}$

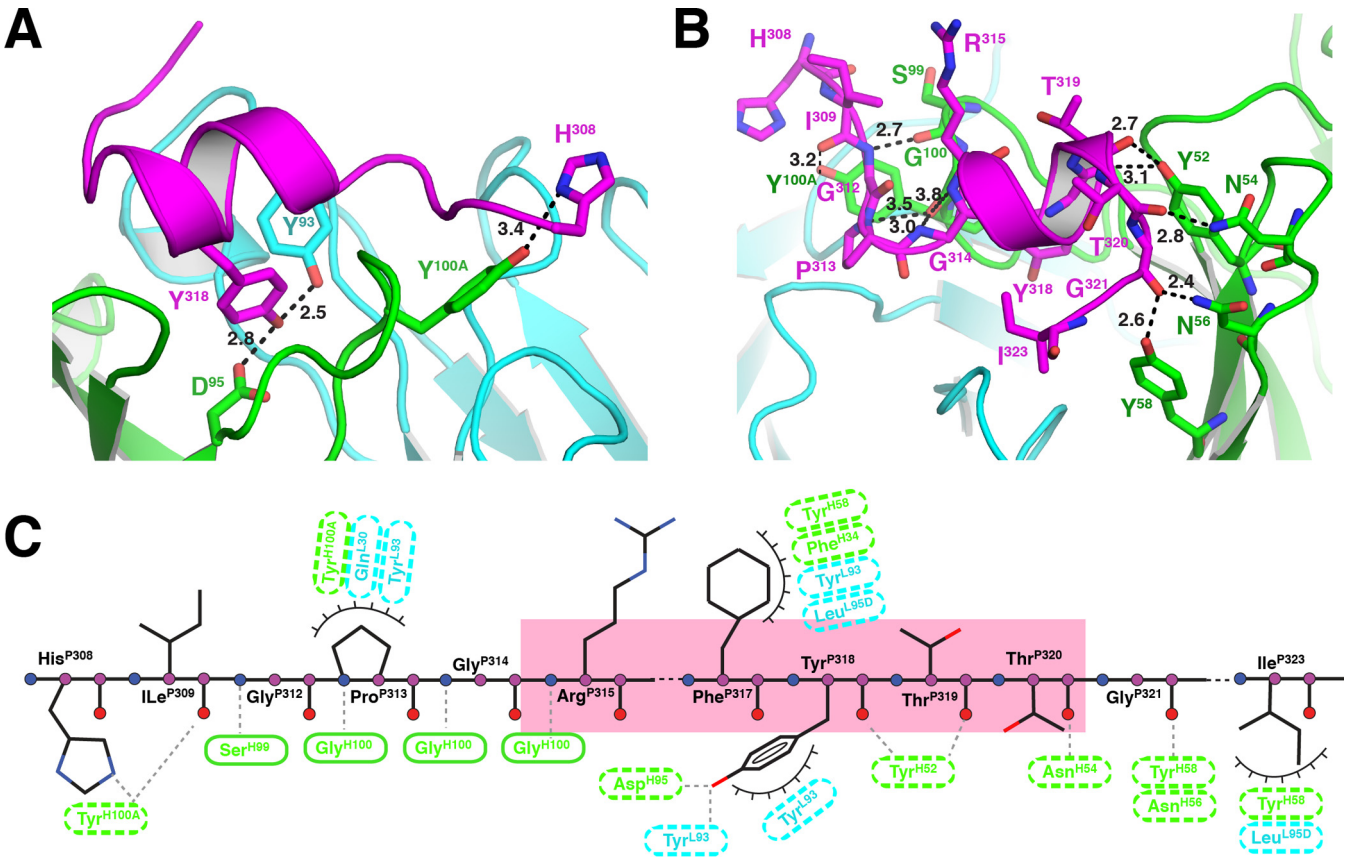


**FIG 4** Antigen-antibody interactions of 10A37/$V3_{JR-FL}$. (A) Hydrophilic interactions between the side chains of epitope and residues of 10A37. (B) Hydrophilic interactions between the main chains of the epitope and residues of 10A37. (C) Schematic illustration of antigen-antibody interactions. The helix in the epitope is indicated by pink shading.

is buried in a smaller hydrophobic pocket formed by residues $Gln^{L30}$ (L1), $Tyr^{L93}$ (L3), and $Tyr^{H100A}$ (H3). Additional contacts between $Tyr^{P318}$ and $Try^{L93}$ (L3), together with intrachain interactions between $Phe^{P317}$, $Ile^{P323}$, and $Tyr^{P318}$, strengthen overall hydrophobic interactions. Interestingly, $Arg^{P315}$ and $Thr^{P319}$ of $V3_{JR-FL}$, the two residues different from those of the gp120 used as the immunogen to elicit 10A37, only use their backbone to contact antibody. There are 10 main-chain interactions between the backbones of V3 and 10A37, making a notable contribution to the way 10A37 grasps its V3 epitope (Fig. 4B).

**Comparison of the antigen-antibody interactions of rabbit V3 MAbs 10A3 and R56.** The binding mode of 10A3 is very similar to that of another rabbit V3 MAb, R56; they both recognize the crown of V3, mimicking the cradle binding mode of human V3 MAbs derived from the IGHV5-51 germ line gene (Fig. 5) (26). Interestingly, the light chains of 10A3 and R56 are derived from the same rabbit light-chain germ line gene (IGKV1S15*01), although their heavy chains are derived from genes of different germ lines (IGHV1S45*01 and IGHV1S40*01, respectively) (Fig. 5C) (15). The light-chain backbone structures of the two antibodies superimposed remarkably well (C$\alpha$ RMSD, 0.5 Å) (Fig. 5A). In terms of CDRs, 10A3 and R56 are similar to each other with respect to CDRs H3, L1, L2, and L3. Both MAbs have a short 4-residue (Kabat definition) CDR H3 with similar sequence: NFYL (10A3) and NFDL (R56). Sequence alignment analyses show the parallel evolution of 10A3 and R56 during affinity maturation (Fig. 5C). Within the VL gene, there were six identical mutations on both 10A3 and R56 that diverged from the germ line sequence (Gly to $Val^{L3}$, Pro to $Leu^{L4}$, Thr to $Ser^{L25}$, Glu to $Gln^{L27}$, Phe to $Val^{L27B}$, and Ile to $Asn^{L32}$; numbering based on 10A3). Within CDR L3, two residues had identical mutations (Gln to $Leu^{L89}$ and His to $Asp^{L93}$). Within the VH gene, four sites had

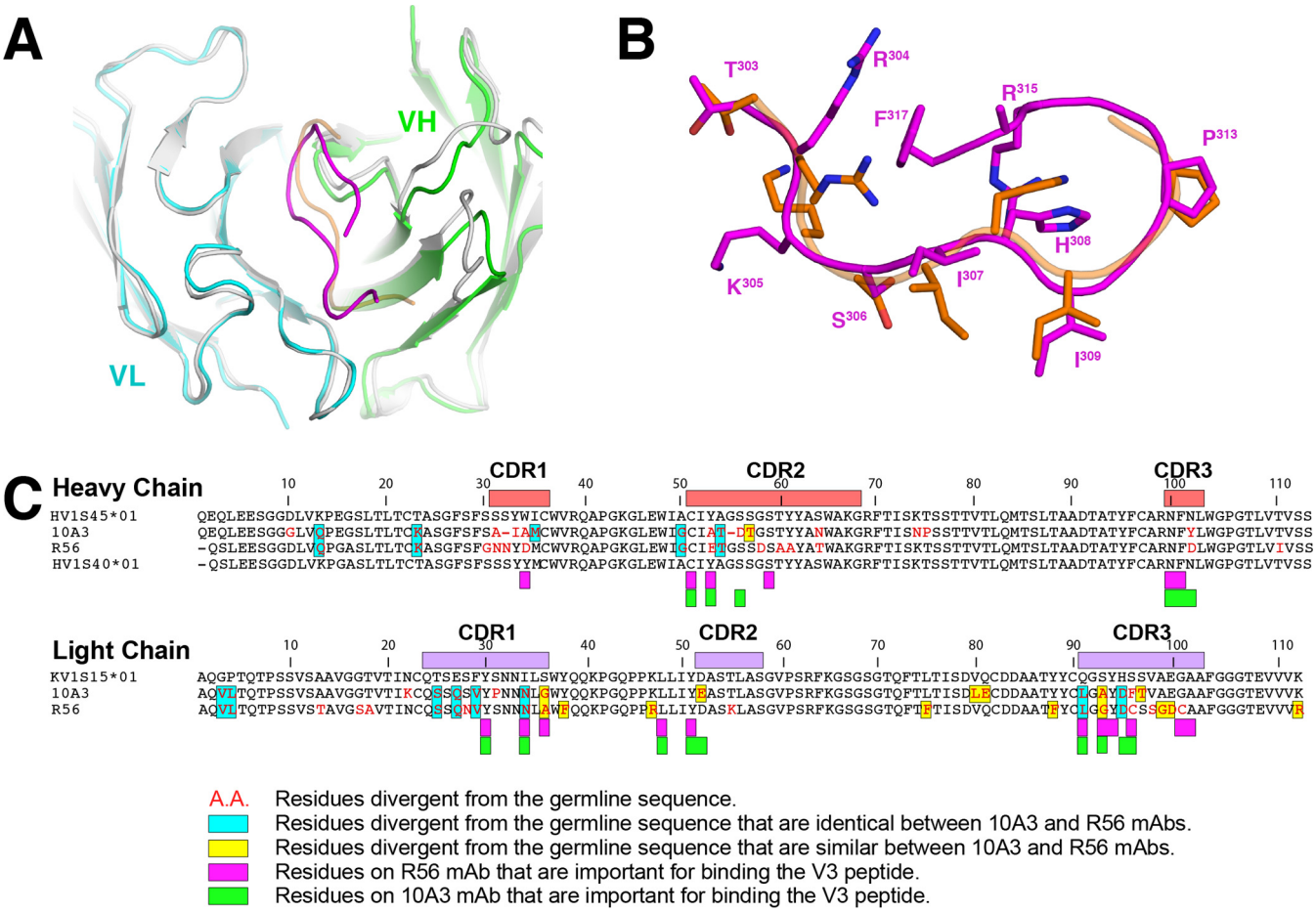


**FIG 5** Structural comparison of rabbit V3 MAb complexes 10A3/$V3_{ConB}$ with R56/$V3_{JR-FL}$. (A) Superimposition of the light-chain variable-domain structures of 10A3/$V3_{ConB}$ and R56/$V3_{JR-FL}$ (C$\alpha$ RMSD, 0.32Å). 10A3 and its epitope are colored as described for Fig. 1. The light and heavy chains of R56 are colored gray, and its epitope is colored orange. (B) Superimposition of the backbone structures of V3 epitopes bound to antibodies 10A3 and R56 with the side chains shown as sticks (C$\alpha$ RMSD, 0.92 Å). (C) Sequence alignment of the heavy (top) and light (bottom) chains of 10A3 and R56 and their germ lines. CDR1, CDR2, and CDR3 are indicated. Critical residues are indicated as shown in the key.

identical mutations (Lys to $Gln^{H13}$, Thr to $Lys^{H23}$, Ala to $Gly^{H49}$, and Ala to $Thr^{H52A}$) and one convergent mutation (Ile to $Met^{H34}$). There were many other mutations in the VL gene, however, most of which were not for residues that make direct contacts with antigens, suggesting their indirect role in shaping the overall paratope conformation.

Not surprisingly, 10A3 and R56 share many common antigen-antibody interactions using identical/similar amino acid residues (Fig. 5C). For the light chain, four of eight positions are conserved, including $Tyr^{L28}$, $Asn^{L32}$, $Tyr^{L49}$, and $Leu^{L89}$. For the heavy chain, three of six residues are identical ($Cys^{H50}$, $Asn^{H95}$, and $Phe^{H96}$). 10A3 and R56 share the N terminus and the arch of the V3 crown as the common epitope region. Two hydrophobic epitope residues, $Ile^{P307}$ and $Ile^{P309}$, are buried in hydrophobic pockets on the antigen binding sites comprised of $Cys^{H50}$, $Leu^{L89}$, and $Phe^{H96}$, while $Pro^{P313}$ stacks against the aromatic plane of $Tyr^{L49}$. In the case of 10A3, the latter interaction is strengthened by $Tyr^{H97}$ that stacks against $Pro^{P313}$ on the opposite side of $Tyr^{L49}$. Two main-chain interactions are also conserved, including $Ile^{P307}$_O and $Asn^{L32}$_ND2 as well as $Gly^{P312}$_N and $Asn^{H95}$_O. Overall, the antigen-antibody interactions are more conserved for the light chain and play a dominant role in antigen binding for both 10A3 and R56, most likely due to their light chains derived from the same germ line gene.

Moreover, the epitope structures of V3 cocrystallized with 10A3 and R56 are very similar (C$\alpha$ RMSD, 0.9 Å) (Fig. 5B), especially at the N terminus and the arch of the V3 crown, a shared epitope region of the two MAbs. The side chains also align very well, except for

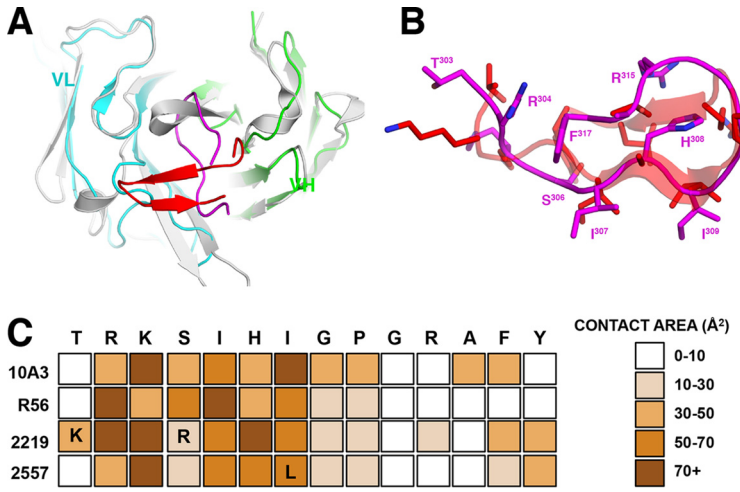


**FIG 6** Structural comparison of rabbit V3 MAb complex 10A3/$V3_{ConB}$ with human V3 MAb complex and others encoded by IGHV5-51 germ line genes. (A) Superimposition of the backbone structures of 10A3/$V3_{ConB}$ and 2557/$V3_{NY5}$ (C$\alpha$ RMSD, 0.94 Å). $V3_{ConB}$ and $V3_{NY5}$ peptides are shown in magenta and red, respectively. 10A3 VL and VH are colored cyan and green, while those of 2557 are colored gray. Note that the V3 epitope bound in different orientations relative to the MAbs. (B) Superimposition of the peptides bound to 10A3 and 2557 with the side chains shown as sticks (C$\alpha$ RMSD, 1.58 Å). (C) Comparison of the V3 epitopes of rabbit and human MAbs. Plot showing the distribution and number of contacts formed with the V3 loop by different MAbs. Squares containing letters indicate peptide differences from that complexed with 10A3, the sequence of which is shown above the grid.

$Arg^{P304}$ and $Lys^{P305}$. However, 10A3 has a longer V3 epitope; it recognizes 13 residues ($^{303}$TRKSIHIGPGRAF$^{317}$), while R56 recognizes only 10 residues ($^{303}$TRKSIHIGPG$^{314}$), i.e., 10A3 epitope has an extension of three more C-terminal residues than R56. Two major factors may have allowed 10A3 to bind the additional three residues: Asp to $Glu^{L50}$ and Ser to $Asp^{H53}$ mutations (Fig. 2A and C). $Glu^{L50}$ potentially can form an extra salt bridge with $Arg^{P315}$ (distance, 3.6 Å) in addition to the close interaction with $His^{P308}$ (2.7 Å), but the side chain of the unmutated germ line $Asp^{L50}$ of R56 is too short to interact with $Arg^{P315}$ (likely >4 Å away). Mutation of Ser to $Asp^{H53}$ allows its side chain to form a salt bridge with $Arg^{P304}$, positioning its guanidinium group to stack with the aromatic plane of $Phe^{P317}$ and further stabilizing the C-terminal end of the V3 crown. In contrast, this is impossible, because $Arg^{P304}$ of V3 forms a buried salt bridge with $Asp^{H34}$ on the surface of R56 (26). Thus, additional mutations in affinity maturation have introduced V3 contacts in 10A3 that are lacking in R56, further stabilizing the C-terminal V3 crown region.

**Comparison of the antigen-antibody interactions of rabbit 10A3 with human IGHV5-51-encoded V3 MAbs.** Crystal structures of several human V3 MAbs derived from IGHV5-51 germ line genes have been determined, including the MAb 2557, a typical human IGHV5-51-encoded V3 MAb (8, 19, 25). They all use the cradle binding mode to bind the V3 crown. The overall conformations of the V3 peptides bound to 10A3 and 2557 are similar, although the V3 epitope recognized by 2557 is one amino acid longer at the C terminus and forms a rather regular two-stranded antiparallel beta sheet, whereas the peptide bound to 10A3 exists as a hairpin coil (Fig. 6A). However, the V3 epitopes of the two antibodies orient nearly perpendicular to each other in relationship to their antigen binding sites. The apex arch of the V3 crown is laid on top of the CDR H3 when complexed with 10A3, while it points toward the CDR L1 when complexed with human MAb 2557. Another difference between the rabbit MAbs 10A3 and R56 and those of human IGHV5-51 V3 MAbs is the extremely short CDR H3; CDR H3 in the rabbit MAbs is buried under the epitope, while the CDR H3 in the human ones forms a wall on one side of the cradle. Nevertheless, the epitope structures of V3 cocrystallized with 10A3 and 2557 are similar (C$\alpha$ RMSD, 1.58 Å) (Fig. 6B), especially at the N terminus and the arch of the V3 crown, the common epitope region for both

antibodies. The C terminus of the MAb-bound V3 crown was more variable than the N terminus, which is the case for all human V3 MAbs derived from IGHV5-51 germ line genes.

Structural analyses show the high similarities between rabbit and human V3 MAbs using the cradle binding mode in general. There is considerable overlap in the distribution and number of contacts formed with the V3 loop by different MAbs (Fig. 6C). A detailed comparison of contact area between the epitopes of rabbit MAbs 10A3 and R56 with those of selected human V3 MAbs 2219 and 2557 shows their similar recognition patterns. First, they all focus on the N terminus of the V3 crown and have very few contacts with the C terminus. Second, positively charged residues at the N terminus of the V3 crown play key roles in the antigen-antibody interaction. Third, $Pro^{P313}$ in the arch region always stacks against aromatic planes. Fourth, V3 residue 315 (often $Arg^{P315}$ and $Gln^{P315}$ for clade B and non-clade B strains, respectively) does not play a significant role in antibody binding. This also explained that we could crystallize 10A3 with a V3 with $Arg^{P315}$, although the antibody was induced by a gp120 with $Gln^{P315}$. In spite of the MAb sequence and underlying germ line differences, it is clear that the rabbit MAbs can recognize the V3 crown in binding modes similar to those of the human MAbs.

## DISCUSSION

In this study, we determined and analyzed Fab/peptide complex structures of two recently isolated rabbit anti-V3 neutralizing MAbs, 10A3 and 10A37, and defined their epitopes at the atomic level. Our results showed that 10A3 recognizes the V3 crown region ($^{303}$TRKSIHIGPGRAF$^{317}$), and 10A37 targets the V3 crown and the succeeding stem region ($^{308}$HIGPGRAFYTTGEI$^{323}$). By and large, 10A3 is similar to previously reported rabbit MAb R56, except that its epitope is longer than that of R56 by three amino acids at its C-terminal end, resulting in a hairpin structure. In contrast and unlike most vaccine-induced V3-specific MAbs, 10A37 targets primarily the C-terminal end of the V3 crown as well as the succeeding stem region, a newly observed V3 binding mode. Moreover, its epitope has an $\alpha$-helix core that has not been previously observed. Early theoretical prediction suggested that V3 can contain a short helix near the C-terminal region of V3 (35), and some nuclear magnetic resonance studies also reported that C-terminal portions of the V3 loop could assume an alpha-helical structure in a trifluoroethanol-water mixture ($^{324}$IGTIRQAHC$^{332}$ [36] and $^{320}$TGEIIGDIR$^{328}$ [37]). However, these helical conformations were observed under unusual buffer conditions and are downstream of the helical region observed in our crystal structure, $^{315}$RAFYTT$^{320}$.

The epitope of 10A3 and its interaction with the V3 crown is an example demonstrating the increased complexity of an antibody's epitope correlating with its affinity maturation (26). In the case of rabbit MAb R56, which has a V3 binding mode very similar to that of 10A3 (Fig. 5), only the first half of the V3 crown was observed when it is in complex with R56. Since the V3 crown has the propensity to form a beta hairpin (6, 9, 38), the C-terminal half of the crown likely is located spatially next to the N-terminal half. However, R56 has not developed contact that can stabilize the C-terminal half of the V3 crown and therefore could not be observed in the R56/V3 structure. However, in the case of 10A3, contacts have been developed through additional somatic hypermutations, and these contacts further stabilize the C-terminal half of the V3 crown, allowing it to be observed in 10A3/V3 complex structure. We have only speculated previously about this relationship between affinity maturation and the complexity of an antibody's epitope (26), but here we have demonstrated that, by the complex structure of rabbit MAb 10A3, 10A3 has a binding mode essentially identical to that of R56 but with additional somatic hypermutations. These additional hypermutations may provide an explanation for the improved neutralization potency of 10A3 (Table 2). Together with R56, our results for 10A3 further support the notion that rabbit antibodies can mimic the binding modes of human antibodies, at least against the V3 crown. This similarity is likely predetermined by the structure of the V3 crown and its

**TABLE 2** Neutralizing activities of MAbs in a TZM-bl assay[a]

| | $IC_{50}$ ($\mu$g/ml) for: | | | | | | | |
|---|---|---|---|---|---|---|---|---|
| MAb | SF162 | Ss1196 | QH0692 | Bx08.16 | W61D-TCLA.71 | BaL.26 | MW965.26 | 92BR025.9 |
| R56 | 0.1 | 7.18 | 8.6 | 3.18 | ND | 2.07 | <0.02 | ND |
| 10A3 | 0.05 | 5.51 | ND | 1.9 | <0.01 | 1.06 | <0.02 | 39.2 |

[a]See references 15 and 16. ND, not determined.

immunogenicity. Human antibodies encoded by IGHV5-51 have an antigen binding site that can best accommodate the beta hairpin structure of the V3 crown, burying the N-terminal half of the V3 crown in the cradle-like binding site. The immunodominance of the V3 crown and the ideal shape for the cradle binding site can then explain the preferential gene usage of IGHV5-51 (19). Thus, it is not surprising that rabbit can mount immune responses against the V3 crown and produce antibodies with a binding mode similar to those of human antibodies.

Our structure of the 10A37 complex demonstrates that the C-terminal end of the V3 crown can have a helical conformation different from the commonly observed beta strand. In all of the currently available Env trimer structures, including the high-resolution cryoelectron microscopy structure of the JR-FL trimer, this region has a beta strand conformation, suggesting that the beta strand is the preferred structure in the prefusion trimer. However, V3 loops tend to flick out easily (39, 40), and this region may become accessible for antibody binding; it can be a vulnerable site for immune responses, because the C-terminal end of the V3 crown is quite conserved in sequence (8), and the possibility of multiple structural conformations can be a mechanism for masking this region (41). Our structural data also explain the breadth of 10A37 in neutralization (16). Although 10A37 has a deep pocket for binding the side chains of $Phe^{P317}$ and $Tyr^{P318}$ and thus is side chain specific, these two residues are highly conserved in HIV strains (8). In addition, the rest of the antibody-V3 interactions are largely backbone contacts, which are not influenced much by sequence variations. Interestingly, 10A3 and 10A37 have similar binding affinities (not shown), and we speculate the difference in the breadth is due to the difference in the target epitopes.

In conclusion, our study provides novel insights about neutralization-susceptible epitope structures of the V3 loop of gp120 and more evidence that, despite low amino acid sequence similarity with human antibody germ line genes, rabbits can serve as a useful animal model to evaluate human vaccine candidates.

## MATERIALS AND METHODS

**Fab production and purification.** MAbs 10A3 and 10A37 were expressed and purified as previously described (16). Briefly, plasmids encoding the heavy and light chains were transfected into 293F cells using 293fectin (Invitrogen). The cell culture supernatant was collected 5 days after transfection and clarified by centrifugation. The MAbs then were purified using a protein A column, eluted, and dialyzed in phosphate-buffered saline (PBS).

The Fab fragments of rabbit MAbs were prepared by papain digestion as described previously (24). Briefly, the IgG molecule was mixed with papain (Worthington, Lakewood, NJ) at a 20:1 molar ratio in 100 mM Tris (pH 6.8) with 1 mM cysteine hydrochloride and 4 mM EDTA. The mixture was incubated for 1 h at 37°C, and the reaction was stopped by 10 mM iodoacetamide. The Fab fragment was separated from the Fc fragment and the undigested IgG by a protein A column and further purified by size exclusion chromatography. The Fab fragment then was concentrated to about 10 mg/ml for crystallization.

**Crystallization, data collection, structure determination, and refinement.** The $V3_{ConB}$ peptide obtained from the NIH AIDS Reagent Program and the $V3_{JR\text{-}FL}$ peptide, synthesized by Biomatik (Wilmington, DE), were dissolved in water and dimethyl sulfoxide (DMSO), respectively, and mixed with Fabs 10A3 and 10A37 at a 10:1 molar ratio. Crystallization conditions were screened and optimized using the vapor diffusion hanging-drop method. Well-diffracted crystals of 10A3 Fab/$V3_{ConB}$ complex were obtained with a well solution of 32% polyethylene glycol 6000, 1 M LiCl, 0.1 M Tris, pH 8.0, whereas those of the 10A37 Fab/$V3_{JR\text{-}FL}$ complex were obtained in a well solution of 18% polyethylene glycol 4000, 8.5% isopropanol, 0.1 M HEPES, pH 7.5, 15% glycerol. X-ray diffraction data sets were collected at beam lines X6A and X4A, National Synchrotron Light Source (NSLS), Brookhaven National Laboratory. All data sets were processed using the HKL2000 package (42) and XDS (43), and structures were determined by molecular replacement using the R56 Fab structure (PDB entry 4JO1) as the initial model. Cycles of refinement for each model were carried out in COOT (44) and PHENIX (45). Coordinates and structure factors of 10A3/$V3_{ConB}$ and 10A37/$V3_{JR\text{-}FL}$ complexes have been deposited in the Protein Data Bank.

**Comparative analyses of rabbit and human MAbs.** Structural analyses were carried out using ICM (46), and figures were generated using PyMOL (http://pymol.org). The antigen-antibody interactions described in figures were calculated by ICM and PDBePISA (EMBL-EBI). For comparison with rabbit MAbs 10A3 and R56, two V3 human MAbs were chosen that are encoded by IGHV5-51 germ line genes: MAbs 2219 and 2557 (PDB entries 2B0S and 3MLT). Human antibodies binding to V3 using different binding modes or binding to other parts of the V3 loop, or to V3 loops with highly dissimilar sequences, have been omitted from this analysis.

**Accession number(s).** PDB entries for the 10A37 and 10A3 structures are 5V6L and 5V6M, respectively.

## ACKNOWLEDGMENTS

We thank staff members at beam lines X6A and X4A, NSLS, for their help with X-ray diffraction data collection and Michael Wuo and Bobby Arora for help with the CD experiments.

This work was supported by funding from Iowa State University and NIH grants AI074286 and AI100151.

HIV consensus subtype B Env (15-mer) peptide was obtained through the AIDS Research and Reference Reagent Program, Division of AIDS, NIAID, NIH.

M.W.C. has an equity interest in NeoVaxSyn, Inc., and serves as the CEO/president. However, NeoVaxSyn Inc. did not contribute to this work or the interpretation of the data.

## REFERENCES

1. McKeating JA, Gow J, Goudsmit J, Pearl LH, Mulder C, Weiss RA. 1989. Characterization of HIV-1 neutralization escape mutants. AIDS 3:777–784. https://doi.org/10.1097/00002030-198912000-00001.
2. Ivanoff LA, Dubay JW, Morris JF, Roberts SJ, Gutshall L, Sternberg EJ, Hunter E, Matthews TJ, Petteway SR, Jr. 1992. V3 loop region of the HIV-1 gp120 envelope protein is essential for virus infectivity. Virology 187:423–432. https://doi.org/10.1016/0042-6822(92)90444-T.
3. Wyatt R, Kwong PD, Desjardins E, Sweet RW, Robinson J, Hendrickson WA, Sodroski JG. 1998. The antigenic structure of the HIV gp120 envelope glycoprotein. Nature 393:705–711. https://doi.org/10.1038/31514.
4. Resch W, Hoffman N, Swanstrom R. 2001. Improved success of phenotype prediction of the human immunodeficiency virus type 1 from envelope variable loop 3 sequence using neural networks. Virology 288:51–62. https://doi.org/10.1006/viro.2001.1087.
5. Leonard CK, Spellman MW, Riddle L, Harris RJ, Thomas JN, Gregory TJ. 1990. Assignment of intrachain disulfide bonds and characterization of potential glycosylation sites of the type 1 recombinant human immunodeficiency virus envelope glycoprotein (gp120) expressed in Chinese hamster ovary cells. J Biol Chem 265:10373–10382.
6. Huang CC, Tang M, Zhang MY, Majeed S, Montabana E, Stanfield RL, Dimitrov DS, Korber B, Sodroski J, Wilson IA, Wyatt R, Kwong PD. 2005. Structure of a V3-containing HIV-1 gp120 core. Science 310:1025–1028. https://doi.org/10.1126/science.1118398.
7. Huang CC, Lam SN, Acharya P, Tang M, Xiang SH, Hussan SS, Stanfield RL, Robinson J, Sodroski J, Wilson IA, Wyatt R, Bewley CA, Kwong PD. 2007. Structures of the CCR5 N terminus and of a tyrosine-sulfated antibody with HIV-1 gp120 and CD4. Science 317:1930–1934. https://doi.org/10.1126/science.1145373.
8. Jiang X, Burke V, Totrov M, Williams C, Cardozo T, Gorny MK, Zolla-Pazner S, Kong XP. 2010. Conserved structural elements in the V3 crown of HIV-1 gp120. Nat Struct Mol Biol 17:955–961. https://doi.org/10.1038/nsmb.1861.
9. Pancera M, Zhou T, Druz A, Georgiev IS, Soto C, Gorman J, Huang J, Acharya P, Chuang GY, Ofek G, Stewart-Jones GB, Stuckey J, Bailer RT, Joyce MG, Louder MK, Tumba N, Yang Y, Zhang B, Cohen MS, Haynes BF, Mascola JR, Morris L, Munro JB, Blanchard SC, Mothes W, Connors M, Kwong PD. 2014. Structure and immune recognition of trimeric pre-fusion HIV-1 Env. Nature 514:455–461. https://doi.org/10.1038/nature13808.
10. Zwart G, Langedijk H, van der Hoek L, de Jong JJ, Wolfs TF, Ramautarsing C, Bakker M, de Ronde A, Goudsmit J. 1991. Immunodominance and antigenic variation of the principal neutralization domain of HIV-1. Virology 181:481–489. https://doi.org/10.1016/0042-6822(91)90880-K.
11. Gorny MK, Xu J-Y, Karwowska S, Buchbinder A, Zolla-Pazner S. 1993. Repertoire of neutralizing human monoclonal antibodies specific for the V3 domain of HIV-1 gp120. J Immunol 150:635–643.
12. Ghiara JB, Stura EA, Stanfield RL, Profy AT, Wilson IA. 1994. Crystal structure of the principal neutralization site of HIV-1. Science 264:82–85. https://doi.org/10.1126/science.7511253.
13. Zolla-Pazner S. 2004. Identifying epitopes of HIV-1 that induce protective antibodies. Nat Rev Immunol 4:199–210. https://doi.org/10.1038/nri1307.
14. Laman JD, Schellekens MM, Lewis GK, Moore JP, Matthews TJ, Langedijk JP, Meloen RH, Boersma WJ, Claassen E. 1993. A hidden region in the third variable domain of HIV-1 IIIB gp120 identified by a monoclonal antibody. AIDS Res Hum Retrovir 9:605–612. https://doi.org/10.1089/aid.1993.9.605.
15. Chen Y, Vaine M, Wallace A, Han D, Wan S, Seaman MS, Montefiori D, Wang S, Lu S. 2013. A novel rabbit monoclonal antibody platform to dissect the diverse repertoire of antibody epitopes for HIV-1 Env immunogen design. J Virol 87:10232–10243. https://doi.org/10.1128/JVI.00837-13.
16. Qin Y, Banerjee S, Agrawal A, Shi H, Banasik M, Lin F, Rohl K, LaBranche C, Montefiori DC, Cho MW. 2015. Characterization of a large panel of rabbit monoclonal antibodies against HIV-1 gp120 and isolation of novel neutralizing antibodies against the V3 loop. PLoS One 10:e0128823. https://doi.org/10.1371/journal.pone.0128823.
17. Hessell AJ, McBurney S, Pandey S, Sutton W, Liu L, Li L, Totrov M, Zolla-Pazner S, Haigwood NL, Gorny MK. 2016. Induction of neutralizing antibodies in rhesus macaques using V3 mimotope peptides. Vaccine 34:2713–2721. https://doi.org/10.1016/j.vaccine.2016.04.027.
18. Balasubramanian P, Kumar R, Williams C, Itri V, Wang S, Lu S, Hessell AJ, Haigwood NL, Sinangil F, Higgins KW, Liu L, Li L, Nyambi P, Gorny MK, Totrov M, Nadas A, Kong XP, Zolla-Pazner S, Hioe CE. 2017. Differential induction of anti-V3 crown antibodies with cradle- and ladle-binding modes in response to HIV-1 envelope vaccination. Vaccine 35:1464–1473. https://doi.org/10.1016/j.vaccine.2016.11.107.
19. Gorny MK, Wang XH, Williams C, Volsky B, Revesz K, Witover B, Burda S, Urbanski M, Nyambi P, Krachmarov C, Pinter A, Zolla-Pazner S, Nadas A. 2009. Preferential use of the VH5-51 gene segment by the human immune response to code for antibodies against the V3 domain of HIV-1. Mol Immunol 46:917–926. https://doi.org/10.1016/j.molimm.2008.09.005.
20. Rini JM, Stanfield RL, Stura EA, Salinas PA, Profy AT, Wilson IA. 1993. Crystal structure of a human immunodeficiency virus type 1 neutralizing antibody, 50.1, in complex with its V3 loop peptide antigen. Proc Natl Acad Sci U S A 90:6325–6329. https://doi.org/10.1073/pnas.90.13.6325.
21. Stanfield RL, Gorny MK, Williams C, Zolla-Pazner S, Wilson IA. 2004. Structural rationale for the broad neutralization of HIV-1 by human

monoclonal antibody 447-52D. Structure 12:193–204. https://doi.org/10.1016/j.str.2004.01.003.
22. Stanfield RL, Gorny MK, Zolla-Pazner S, Wilson IA. 2006. Crystal structures of human immunodeficiency virus type 1 (HIV-1) neutralizing antibody 2219 in complex with three different V3 peptides reveal a new binding mode for HIV-1 cross-reactivity. J Virol 80:6093–6105. https://doi.org/10.1128/JVI.00205-06.
23. Bell CH, Pantophlet R, Schiefner A, Cavacini LA, Stanfield RL, Burton DR, Wilson IA. 2008. Structure of antibody F425-B4e8 in complex with a V3 peptide reveals a new binding mode for HIV-1 neutralization. J Mol Biol 375:969–978. https://doi.org/10.1016/j.jmb.2007.11.013.
24. Burke V, Williams C, Sukumaran M, Kim S, Li H, Wang X-H, Gorny MK, Zolla-Pazner S, Kong X-P. 2009. Structural basis of the cross-reactivity of genetically related human anti-HIV-1 mAbs: implications for design of V3-based immunogens. Structure 17:1538–1546. https://doi.org/10.1016/j.str.2009.09.012.
25. Gorny MK, Sampson J, Li H, Jiang X, Totrov M, Wang XH, Williams C, O'Neal T, Volsky B, Li L, Cardozo T, Nyambi P, Zolla-Pazner S, Kong XP. 2011. Human anti-V3 HIV-1 monoclonal antibodies encoded by the VH5-51/VL lambda genes define a conserved antigenic structure. PLoS One 6:e27780. https://doi.org/10.1371/journal.pone.0027780.
26. Pan R, Sampson JM, Chen Y, Vaine M, Wang S, Lu S, Kong XP. 2013. Rabbit anti-HIV-1 monoclonal antibodies raised by immunization can mimic the antigen-binding modes of antibodies derived from HIV-1-infected humans. J Virol 87:10221–10231. https://doi.org/10.1128/JVI.00843-13.
27. Gottardo R, Bailer RT, Korber BT, Gnanakaran S, Phillips J, Shen X, Tomaras GD, Turk E, Imholte G, Eckler L, Wenschuh H, Zerweck J, Greene K, Gao H, Berman PW, Francis D, Sinangil F, Lee C, Nitayaphan S, Rerks-Ngarm S, Kaewkungwal J, Pitisuttithum P, Tartaglia J, Robb ML, Michael NL, Kim JH, Zolla-Pazner S, Haynes BF, Mascola JR, Self S, Gilbert P, Montefiori DC. 2013. Plasma IgG to linear epitopes in the V2 and V3 regions of HIV-1 gp120 correlate with a reduced risk of infection in the RV144 vaccine efficacy trial. PLoS One 8:e75665. https://doi.org/10.1371/journal.pone.0075665.
28. Zolla-Pazner S, Edlefsen PT, Rolland M, Kong XP, deCamp A, Gottardo R, Williams C, Tovanabutra S, Sharpe-Cohen S, Mullins JI, deSouza MS, Karasavvas N, Nitayaphan S, Rerks-Ngarm S, Pitisuttihum P, Kaewkungwal J, O'Connell RJ, Robb ML, Michael NL, Kim JH, Gilbert P. 2014. Vaccine-induced human antibodies specific for the third variable region of HIV-1 gp120 impose immune pressure on infecting viruses. EBioMedicine 1:37–45. https://doi.org/10.1016/j.ebiom.2014.10.022.
29. Dhillon AK, Stanfield RL, Gorny MK, Williams C, Zolla-Pazner S, Wilson IA. 2008. Structure determination of an anti-HIV-1 Fab 447-52D-peptide complex from an epitaxially twinned data set. Acta Crystallogr D Biol Crystallogr 64:792–802. https://doi.org/10.1107/S0907444908013978.
30. Killikelly A, Zhang HT, Spurrier B, Williams C, Gorny MK, Zolla-Pazner S, Kong XP. 2013. Thermodynamic signatures of the antigen binding site of mAb 447-52D targeting the third variable region of HIV-1 gp120. Biochemistry 52:6249–6257. https://doi.org/10.1021/bi400645e.
31. Walker LM, Huber M, Doores KJ, Falkowska E, Pejchal R, Julien JP, Wang SK, Ramos A, Chan-Hui PY, Moyle M, Mitcham JL, Hammond PW, Olsen OA, Phung P, Fling S, Wong CH, Phogat S, Wrin T, Simek MD, Koff WC, Wilson IA, Burton DR, Poignard P. 2011. Broad neutralization coverage of HIV by multiple highly potent antibodies. Nature 477:466–470. https://doi.org/10.1038/nature10373.
32. Abhinandan KR, Martin AC. 2008. Analysis and improvements to Kabat and structurally correct numbering of antibody variable domains. Mol Immunol 45:3832–3839. https://doi.org/10.1016/j.molimm.2008.05.022.
33. Pan R, Chen Y, Vaine M, Hu G, Wang S, Lu S, Kong XP. 2015. Structural analysis of a novel rabbit monoclonal antibody R53 targeting an epitope in HIV-1 gp120 C4 region critical for receptor and co-receptor binding. Emerg Microbes Infect 4:e44. https://doi.org/10.1038/emi.2015.44.
34. Stanfield RL, Wilson IA. 2005. Structural studies of human HIV-1 V3 antibodies. Hum Antibodies 14:73–80.
35. LaRosa GJ, Davide JP, Weinhold K, Waterbury JA, Profy AT, Lewis JA, Langlois AJ, Dreesman GR, Boswell RN, Shadduck P, Holley LH, Karplus M, Bolognesi DP, Mathews TJ, Emini EA, Putney SD. 1990. Conserved sequence and structural elements in the HIV-1 principal neutralizing determinant. Science 249:932–935. https://doi.org/10.1126/science.2392685.
36. Catasti P, Fontenot JD, Bradbury EM, Gupta G. 1995. Local and global structural properties of the HIV-MN V3 loop. J Biol Chem 270:2224–2232. https://doi.org/10.1074/jbc.270.5.2224.
37. Vranken WF, Budesinsky M, Fant F, Boulez K, Borremans FA. 1995. The complete consensus V3 loop peptide of the envelope protein gp120 of HIV-1 shows pronounced helical character in solution. FEBS Lett 374:117–121. https://doi.org/10.1016/0014-5793(95)01086-T.
38. Julien JP, Cupo A, Sok D, Stanfield RL, Lyumkis D, Deller MC, Klasse PJ, Burton DR, Sanders RW, Moore JP, Ward AB, Wilson IA. 2013. Crystal structure of a soluble cleaved HIV-1 envelope trimer. Science 342:1477–1483. https://doi.org/10.1126/science.1245625.
39. Kwon YD, Pancera M, Acharya P, Georgiev IS, Crooks ET, Gorman J, Joyce MG, Guttman M, Ma X, Narpala S, Soto C, Terry DS, Yang Y, Zhou T, Ahlsen G, Bailer RT, Chambers M, Chuang GY, Doria-Rose NA, Druz A, Hallen MA, Harned A, Kirys T, Louder MK, O'Dell S, Ofek G, Osawa K, Prabhakaran M, Sastry M, Stewart-Jones GB, Stuckey J, Thomas PV, Tittley T, Williams C, Zhang B, Zhao H, Zhou Z, Donald BR, Lee LK, Zolla-Pazner S, Baxa U, Schon A, Freire E, Shapiro L, Lee KK, Arthos J, Munro JB, Blanchard SC, Mothes W, Binley JM, McDermott AB, Mascola JR, Kwong PD. 2015. Crystal structure, conformational fixation and entry-related interactions of mature ligand-free HIV-1 Env. Nat Struct Mol Biol 22:522–531. https://doi.org/10.1038/nsmb.3051.
40. Zolla-Pazner S, Cohen SS, Boyd D, Kong XP, Seaman M, Nussenzweig M, Klein F, Overbaugh J, Totrov M. 2015. Structure/function studies involving the V3 region of the HIV-1 envelope delineate multiple factors that affect neutralization sensitivity. J Virol 90:636–649. https://doi.org/10.1128/JVI.01645-15.
41. Kwong PD, Doyle ML, Casper DJ, Cicala C, Leavitt SA, Majeed S, Steenbeke TD, Venturi M, Chaiken I, Fung M, Katinger H, Parren PW, Robinson J, Van Ryk D, Wang L, Burton DR, Freire E, Wyatt R, Sodroski J, Hendrickson WA, Arthos J. 2002. HIV-1 evades antibody-mediated neutralization through conformational masking of receptor-binding sites. Nature 420:678–682. https://doi.org/10.1038/nature01188.
42. Otwinowski Z, Minor W. 1997. Processing of X-ray diffraction data collected in oscillation mode. Methods Enzymol 276:307–326. https://doi.org/10.1016/S0076-6879(97)76066-X.
43. Kabsch W. 2010. Xds. Acta Crystallogr D Biol Crystallogr 66:125–132. https://doi.org/10.1107/S0907444909047337.
44. Emsley P, Cowtan K. 2004. COOT: model-building tools for molecular graphics. Acta Crystallogr D Biol Crystallogr 60:2126–2132. https://doi.org/10.1107/S0907444904019158.
45. Adams PD, Grosse-Kunstleve RW, Hung LW, Ioerger TR, McCoy AJ, Moriarty NW, Read RJ, Sacchettini JC, Sauter NK, Terwilliger TC. 2002. PHENIX: building new software for automated crystallographic structure determination. Acta Crystallogr D Biol Crystallogr 58:1948–1954. https://doi.org/10.1107/S0907444902016657.
46. Abagyan RA, Totrov M, Kuznetsov D. 1994. ICM–a new method for protein modeling and design: applications to docking and structure prediction from the distorted native conformation. J Comput Chem 15:488–506. https://doi.org/10.1002/jcc.540150503.